p38MAPK/p53 signaling axis mediates neuronal apoptosis in response to tetrahydrobiopterin-induced oxidative stress and glucose uptake inhibition: implication for neurodegeneration

Simone Cardaci, Giuseppe Filomeni, Giuseppe Rotilio, Maria R Ciriolo

p38^{MAPK}/p53 signaling axis mediates neuronal apoptosis in response to tetrahydrobiopterin-induced oxidative stress and glucose uptake inhibition: implication for neurodegeneration

Simone Cardaci[*,†], Giuseppe Filomeni[*,†], Giuseppe Rotilio[†,‡], and Maria R. Ciriolo[†,‡,§].

From: [†]Department of Biology, University of Rome "Tor Vergata", Via della Ricerca Scientifica, 1, 00133 Rome, Italy.
[‡]Research Centre IRCCS San Raffaele - Pisana, Via dei Bonacolsi, 00163, Rome, Italy.
[*]Both authors contributed equally to this work.
Page heading title: p38^{MAPK}/p53 role in BH4-induced oxidative/energetic stress.
[§]Address correspondence to: Maria Rosa Ciriolo, Department of Biology, University of Rome "Tor Vergata", Via della Ricerca Scientifica, 00133 Rome, Italy. Phone: +39 06 7259 4369 Fax: +39 06 7259 4311. E-mail: ciriolo@bio.uniroma2.it

Keywords: MAPK, p53, glucose, ROS, glutathione, apoptosis

SYNOPSIS

Tetrahydrobiopterin (BH4) induces neuronal demise *via* production of reactive oxygen species (ROS). Here we investigated the mechanisms of its toxicity and the redox signaling events responsible for the apoptotic commitment in SH-SY5Y neuroblastoma cells and in mouse primary cortical neurons. We identified in $p38^{MAPK}$/p53 a BH4-responsive pro-apoptotic signaling axis, as demonstrated by the recovery of neuronal viability achieved by gene silencing or pharmacological inhibition of both $p38^{MAPK}$ and p53. BH4 induced oxidative stress was characterized by a decrease in GSH/GSSG ratio, an increase in protein carbonylation and DNA damages. BH4 toxicity and redox-activated apoptotic pathway were counteracted by the H_2O_2-scavengers, catalase and N-acetylcysteine and enhanced by the GSH neo-synthesis inhibitor, buthionine sulfoximine (BSO). We also demonstrated that BH4 impairs glucose uptake and utilization that were prevented by catalase administration. This effect contributes to the neuronal demise, exacerbating BH4-induced nuclear damages and the activation of the pro-apoptotic $p38^{MAPK}$/p53 axis. Inhibition of glucose uptake was also observed upon treatment with 6-hydroxydopamine, another redox-cycling molecule, suggesting a common mechanism of action for auto-oxidizable neurotoxins.

INTRODUCTION

Oxidative stress is considered to be an important pathogenetic factor in several neurodegenerative diseases such as Parkinson's disease (PD) and Alzheimer disease (AD). Because of its high metabolic rate and relatively reduced capacity for cellular regeneration compared with other organs, the brain is believed to be particularly susceptible to the damaging effects of ROS. This vulnerability is highlighted by the accumulation of protein carbonyls and lipid hydroperoxides, as well as the decrease of glutathione (GSH) levels both in experimental models of neurological disorders and in *post-mortem* PD and AD brains [1-3]. One of the main determinants of oxidative-dependent neuronal degeneration is the impairment of neuronal bioenergetics. Although mitochondria are the best defined ATP-producing structures oxidatively affected in several neurological disorders, a growing number of reports indicates that ROS play a pivotal role in the hypometabolism of glucose as well. Positron emission tomography analyses demonstrate that glucose utilization is reduced in several regions of AD and PD brains [4, 5]. Moreover, the decline in glucose metabolism appears before the onset of cognitive deficits and seems to sensitize neurons to further energy deficiency and oxidative damage [6-8].

The involvement of oxidative stress in neuronal demise is strengthened by the activation of pro-apoptotic transcription factors, such as p53 [9]. Particularly, the insensitivity of p53-null mice to the dopaminergic neurotoxin MPTP, as well as the resistance observed in mice treated with the p53 inhibitor pifithrin-α, demonstrate the involvement of p53 in PD pathogenesis [10, 11]. Moreover, a pivotal role in the degeneration of neurons seems to be played by the mitogen-activated protein kinases (MAPK). Indeed, the accumulation of phospho-active c-Jun-N-terminal kinase (JNK) and $p38^{MAPK}$ have been detected in *post-mortem* PD and AD brains, and their pharmacological inhibition induces neuroprotection [12, 13, 14].

The enhanced vulnerability of neurons to pro-oxidant settings is exacerbated by the high concentration of redox-active metals in several brain regions and the presence of neuron-specific molecules such as dopamine and neuromelanine, whose metabolism generates ROS. Among the redox-cycling molecules fundamental for brain metabolism, tetrahydrobiopterin (BH4) plays a pivotal role both in neurons and glial cells acting as cofactor for aromatic L-amino acid hydroxylases and nitric oxide synthase (NOS) in catecholamines and nitric oxide synthesis, respectively. Despite its important physiological functions, recent studies demonstrate the implication of BH4 in neuronal apoptosis. Indeed, the exposure of neuronal cell lines and primary cultured rat neurons to BH4 [15, 16] results in the occurrence of oxidative damages and neuronal cell death, consistent with the current view of parkinsonism. In particular it has been reported that

intrastriatal and intraventricular injections of BH4 induce the preferential loss of dopaminergic cells of the nigro-striatal pathway, combined to a motor deficit related to dopamine depletion [17, 18]. Although intracellular BH4 concentration (estimated to be 100 μM) [19] is not toxic, probably due to the high neuronal reducing environment, extracellular BH4 results to be detrimental for neuron viability. Moreover, BH4 can be over-produced in catecholaminergic cells in response to calcium increase, stress conditions and released from neurons and activated glia [20-22]. Therefore, neurons can be exposed to a relatively high levels of BH4 in the brain, conferring on it physiological relevance in neurodegenerative settings. Although the toxic effects of BH4 seem to be dependent on ROS generated during its autoxidation, as well as during the enzymatic catalysis of tyrosine hydroxylase [23], the molecular mechanisms underlying its toxicity have not been completely characterized yet.

Here we investigated the signaling pathways activated in response to BH4 challenge, in neuronal cells. We demonstrated that BH4, induces inhibition of glucose uptake, as a consequence of its ability to produce ROS. The reduced glucose availability and utilization, contribute to the neuronal demise, exacerbating BH4-induced oxidative stress and the commitment of SH-SY5Y cells and mouse primary cortical neurons to apoptosis *via* the $p38^{MAPK}$/p53 axis activation.

MATERIAL AND METHODS

Materials – BH4 and zVAD-*fmk* was from Alexis (Lausen, Switzerland). Buthionine sulfoximine (BSO), catalase, pifithrin-α, EDTA, EGTA, N-acetylcysteine (NAC), paraformaldehyde, propidium iodide, Triton X-100, N(G)-nitro-L-arginine methyl ester (L-NAME), 7-nitroindazole (7-Ni) and 6-hydroxydopamine (6-OHDA) were from Sigma (St. Louis, MO). Goat anti-mouse and anti-rabbit IgG (H+L)-horseradish peroxidase conjugate was from Bio-Rad Lab. (Hercules, CA). Neurobasal Medium, B27 supplement, 2-[N-(7-nitrobenz-2-oxa-1,3-diazol-4-yl) amino]-2-deoxy-D-glucose (2-NBDG), 2',7'-dichlorodihydrofluorescein diacetate (DCFH-DA), 4,5-diaminofluorescein diacetate (DAF-DA) were from Invitrogen-Molecular Probes. The JNK inhibitor I and II, the $p38^{MAPK}$ inhibitor SB203580 and Hoechst 33342 were from Calbiochem (La Jolla, CA). All other chemicals were obtained from Merck (Darmstadt, Germany).

SH-SY5Y cell culture – Human neuroblastoma SH-SY5Y cell line was purchased from the European Collection of Cell Culture and grown in Dulbecco's modified Eagle's medium (DMEM)-F12 supplemented with 10% fetal calf serum (FCS), 1% penicillin/streptomycin and 1% glutamine. The cells were maintained at 37° C in a 5% CO_2 atmosphere in air and routinely trypsinized, plated at 4 x 10^4/ cm^2 flasks. Cell viability was assessed by Trypan blue exclusion.

Glucose-free culture conditions were achieved according to Bellucci et al. [24]. Briefly, SH-SY5Y cell line was incubated in 15 mM Hepes-buffered Salt Solution (HBSS) pH 7.45, supplemented with 10% FCS, 0.01 mM non-essential amino acids, 1% penicillin/streptomycin and 1% glutamine without glucose. As control, cells were grown in the same medium supplemented with 16 mM glucose, which correspond to the concentration present in DMEM/F12 medium.

Primary mouse cortical neurons – Mouse primary cortical neurons (PCN) were obtained from cerebral cortices of E15 C57BL-6 mice embryos. All the experiments were performed according to the Animal Research Guidelines of the European Communities Council Directive (86/609/EEC). Minced cortices were digested with trypsin (Lonza) 0.25% - EDTA at 37 °C for 7 minutes. Cells were stained with 0.08% trypan blue solution and only viable cells were counted and plated at the density of 1 x 10^5/cm^2 onto poly-D-lysine coated coverlips or multiwell plates in 25 mM glucose-containing MEM medium supplemented with 10% fetal bovine serum, 2 mM glutamine, 0.1 mg/ml gentamicin (Invitrogen). After 1h, the medium was replaced with Neurobasal medium containing antioxidant-free B27 supplement (Invitrogen), 2 mM glutamine and 0.1 mg/ml gentamicin. Cell cultures were kept at 37 °C in a humidified atmosphere containing 5% CO_2. Every 3 days, one third of the medium was replaced up to day 7, time at which the cells were treated. Glucose-free culture

conditions were performed by culturing PCN in HBSS supplemented with B27, 0.01 mM non-essential amminoacids, 1% gentamicin and 1% glutamine without glucose. As control, PCN were grown in the same medium supplemented with 25 mM glucose, which correspond to the concentration present in Neurobasal medium.

Transfections – Transfections – Twenty-four hours after plating, 50% confluent SH-SY5Y cells were transfected, with two alternative siRNAs duplex directed against the p53 mRNA target sequence provided respectively by MWG Biotech, Ebersberg, Germany (sip53) and Thermo Fisher Scientific – Dharmacon, Lafayette, CO (sip53-2). Similarly, $p38^{MAPK}$ knock-down was achieved tranfecting the cells with a SignalSilence® Pool $p38^{MAPK}$ siRNA (Cell Signaling Technology, Beverly, MA) (sip38^{MAPK}) or with an ON-TARGET*plus* $p38^{MAPK}$ siRNA (Thermo Fisher Scientific – Dharmacon, Lafayette, CO) (sip38-2). Control cells were transfected with two different scramble siRNAs duplex (siScr and siScr-2), which do not present homology with any other human mRNAs. Plasmids transfections were performed with a pcDNA3 empty vector or with a pcDNA3 vector containing the flag-tagged coding sequence for the α1 subunit of $p38^{MAPK}$ carrying the replacement of the Thr^{180} and Tyr^{182} with two non-phosphorilable residues, alanine and phenylalanine respectively (kindly provided by Prof. Jiahuai Han, from The Scripps Research Institute, Department of Immunology, North Torrex Pines Road, La Jolla, CA, USA). Cell transfection was performed as previously described [25].

Treatments – A 10 mM solution of BH4 was prepared just before the experiments by dissolving the powder in water. Treatments were performed at final concentrations ranging from 0.5 to 200 μM, in medium. As control, equal volumes of water were added to untreated cells. The concentration of 100 μM and 1 μM BH4 were selected for the following experiments in SH-SY5Y cells and PCN respectively, if not otherwise indicated, because they allowed the evaluation of a reliable apoptotic degree in a time-window of 24 h. The pan-caspase inhibitor zVAD-*fmk* and the p53 inhibitor pifithrin-α were used at 20 μM, pre-incubated for 1 h before the addition of BH4, and maintained throughout the experiment. BSO was used at the final concentration of 1 mM or 25 μM in SH-SY5Y cells and PCN respectively, added 12 h before BH4 addition and maintained throughout the experiment. The JNK inhibitor I and II were used at the concentration of 10 μM. The $p38^{MAPK}$ inhibitor SB203580 was used at the concentration of 15 μM. NAC was used at the final concentration of 5 mM. After 12 h-incubation, the cells were rinsed with PBS and transferred to a fresh NAC-free medium. Catalase (1 μM) was added 1 h before BH4 addition and maintained in the medium throughout the experimental time. Nitric oxide synthase (NOS) inhibitors L-NAME and 7-Ni were used at the concentration of 100 μM and 10 μM respectively, pre-incubated for 1h before BH4 addition and maintained throughout the experiment.

Analysis of cell viability and apoptosis – Adherent (after trypsinization) and detached SH-SY5Y cells were combined, washed with PBS and stained with 50 μg/ml propidium iodide prior to analysis by a FACScalibur instrument (Becton Dickinson, San Josè, CA). The percentages of apoptotic cells were evaluated according to Nicoletti et al. [26]. Determination of PCN apoptosis was performed evaluating nuclear morphology by fluorescence microscopy after incubation with the cell permeable dye Hoechst 33342. The percentages of apoptotic cells were evaluated by counting nuclei displaying condensed or fragmented chromatin in six subfields of each culture. All experiments were performed at least three times with similar results.

Measurement of NO levels – Intracellular NO production was determined by flow cytometry using the cell permeable NO-specific probe 4,5-diaminofluorescein diacetate (DAF-DA, Molecular Probes) according to the manufacturer's instructions.

Western blot analyses – Total protein extracts were obtained as previously described [27]. Protein extracts were then separated by SDS-PAGE and blotted onto nitrocellulose membrane (Bio-Rad). Monoclonal anti-p53 (clone BP5312), anti-actin (Sigma); anti-phospho-thr172 of AMPK α-subunits, anti-caspase-3 (clone3G2 – Cell Signaling Technology); anti-glyceraldehyde-3-phosphate dehydrogenase (GAPDH), anti-phospho JNK1, anti-phospho c-Jun, anti-poly-ADP ribose polymerase (PARP) (Santa Cruz Biotechnology); and polyclonal anti-AMPK, anti-Bax, anti-JNK,

anti-p38^{MAPK} (Santa Cruz Biotechnology); anti-caspase-9 (Cell Signaling Technology); anti phospho-thr180/tyr182 p38^{MAPK} (Invitrogen) were used as primary antibodies. The specific protein complex, formed upon specific secondary antibody treatment, was identified using a Fluorchem Imaging system (Alpha Innotech, M-Medical, Milano, Italy) after incubation with ChemiGlow chemiluminescence substrate (Alpha Innotech).

Measurement of oxidative stress – Intracellular GSH and GSSG and external plasma-membrane thiols were analyzed as previously described [27]. Detection of intracellular ROS by DCFH-DA, was performed as previously described [28]. Carbonylated proteins were detected using the Oxyblot Kit (Intergen, Purchase, NY) after reaction with 2,4-dinitrophenylhydrazine (DNP) for 15 min at 25 °C. Samples were then resolved by 10% SDS-PAGE and DNP-derivatized proteins were identified by immunoblot using an anti-DNP antibody [29].

Fluorescence microscopy analyses – Cells were plated on chamber slides at $6 \times 10^4/cm^2$, fixed with 4% paraformaldehyde and permeabilized. For the determination of DNA damage, they were washed with PBS, blocked with PBS containing 10% FCS, incubated with a monoclonal anti-ser-139-phosphorylated histone H2A.X antibody (clone JBW301 – Upstate Biotechnology), and further probed with Alexa fluor®-488-conjugated secondary antibody (Invitrogen-Molecular Probes). For the determination of p38^{MAPK} and p53 activation/localization, cells were stained with a polyclonal anti-phospho-thr180/tyr182-p38^{MAPK} antibody and with a monoclonal (Sigma) or polyclonal anti-p53 (Santa Cruz Biotechnology) for SH-SY5Y or PCN, respectively. Slides were further probed with Alexa fluor®-488 and Alexa fluor®-568-conjugated secondary antibodies to visualize P-p38^{MAPK} and p53, respectively. To highlight nuclei, cells were also incubated with the cell permeable DNA dye Hoechst 33342 (Calbiochem-Novabiochem). Images of cells were acquired and digitized with a Delta Vision Restoration Microscopy System (Applied Precision Inc., Issaquah, WA) equipped with an Olympus IX70 fluorescence microscope.

Extracellular lactate assay – Extracellular lactate concentration was assessed as previously described [30].

Measurement of glucose uptake – SH-Y5Y cells and PCN were incubated for the indicated experimental time with 100 μM 2-NBDG, a fluorescent derivative of 2-deoxy-D-glucose, in the presence or absence of 1 μM catalase. Cells were exhaustively washed with PBS to stop 2-NBDG uptake, collected and fluorescence analyzed cytofluorometrically.

Proteins were determined by the method of Lowry et al [31].

Data presentation – All experiments were done at least three different times unless otherwise indicated. Data are expressed as means ± S.D. and significance was assessed by Student's *t* test corrected by Bonferroni's method. Differences with p values < 0.05 were considered significant.

RESULTS

BH4 Elicits a Caspase-Dependent Apoptosis in Neuronal Cells – The cytotoxic effects of BH4 were determined in the neuroblastoma cell line SH-SY5Y. **Fig. 1A** shows cytofluorometric analyses of SH-SY5Y cells treated for 24 h with different concentrations of BH4 (50 - 200 μM). Consistent with data present in the literature [32, 33], a dose-dependent increase in the percentage of apoptotic cells (subG1 region of the histogram) was evidenced. Then, to characterize the apoptotic process, we analyzed caspases activation by Western blot. **Fig. 1B** shows that BH4 treatment induced the cleavage of caspase-9 and caspase-3, as well as the proteolysis of PARP, starting from 6 h of treatment. Moreover, the recovery of cell viability (**Suppl. Fig. 1**) achieved by treating the cells with the pan-caspase inhibitor zVAD-*fmk,* demonstrated that the caspase-mediated apoptosis was the principal mechanism of cell death. In order to corroborate the results of SH-SY5Y cells, we moved on mouse primary cortical neurons (PCN), widely employed to investigate the pro-apoptotic mechanisms of neurotoxic molecules. We treated PCN for 24 h with various concentrations of BH4 (1-50 μM) and analyzed apoptosis engagement by counting condensed and fragmented nuclei upon

Hoechst staining and by evaluating caspase-3 cleavage by fluorescence microscopy. Also in this case, BH4 exhibited a marked neurotoxicity. Indeed, cleaved-caspase-3 and apoptotic nuclei were detectable upon 24 h treatment with 1 μM BH4 **(Fig. 1C and D).** On the basis of these results, the concentrations of 100 μM and 1 μM BH4 were selected for the following experiments in SH-SY5Y cells and PCN, respectively.

BH4-induced Neuronal Apoptosis is a ROS-mediated Event – BH4 is a cofactor of neuronal NOS therefore it has a prominent role in nitric oxide (NO) generation. To assess whether nitrosative stress underlay BH4 toxicity, we treated SH-SY5Y cells with BH4 and cytofluorometrically measured both NO levels and apoptosis upon NOS inhibition with 10 μM 7-Ni or 100 μM L-NAME. Neither increase in NO production nor modulation of cell viability were detectable (data not shown), indicating that NO was not involved in BH4 neurotoxicity. Next, we focused on the capability of BH4 to induce oxidative stress. We measured ROS content cytofluorometrically by incubating SH-SY5Y cells with 5 μM of DHDCF-DA. **Fig. 2A** shows that ROS accumulated intracellularly starting from 30 min of treatment. The rapid kinetics of ROS production prompted us to analyze the content of the tripeptide glutathione. HPLC analyses revealed that both the reduced (GSH) and the oxidized (GSSG) form of glutathione were affected by BH4 treatment in neuroblastoma cells. In particular, as depicted in **Fig 2B**, GSH significantly decreased already at 30 min after BH4 administration, whereas GSSG increased during the treatment, suggesting a buffer role for GSH against ROS-mediated oxidative stress. On the basis of these results, we wondered whether the integrity of proteins and DNA, two well-known targets of ROS-mediated damages, was also affected. DNA damage was evaluated by fluorescence microscopy analyses of the phospho-activation of the DNA double-strand break-sensitive histone H2A.X. **Fig 2C** shows that BH4 treatment caused a time-dependent appearance of discrete nuclear foci indicating the recruiting sites of the DNA repair systems, thus revealing the occurrence of DNA-specific damages. Protein oxidation was assessed by evaluating carbonyl content and protein sulphydryls located at the exofacial side of the plasma-membrane. **Suppl. Fig 2A** shows that proteins were efficiently carbonylated in a time-dependent manner. Also, a marked decrease of reduced thiols occurred upon staining with the impermeant thiol-reacting compound Alexa fluor 488 C5-maleimide (**Suppl. Fig 2B**), confirming the oxidative challenge.

To verify the direct association between BH4-induced oxidative stress and the occurrence of apoptosis, we pre-incubated for 12 h the cells with 5 mM NAC to increase intracellular thiol pool, or with 1 μM catalase, an H_2O_2 dismutating enzyme. We then measured ROS content after 3 h incubation with BH4 as well as apoptotic extent after 24 h-treatment. **Fig. 2D** shows that both the antioxidants prevented ROS production and cell death, even though catalase seemed to be more efficient. Since GSH/GSSG ratio also appeared to be profoundly affected upon BH4 treatment, we induced GSH depletion by 12 h pre-treatment with 1 mM BSO, an irreversible inhibitor of GSH neo-synthesis. **Fig. 2E** shows that GSH depletion resulted in an increased ROS levels and an enhanced vulnerability towards BH4. The involvement of oxidative stress in the induction of apoptosis was also confirmed to be operative in neurons, as demonstrated by the complete recovery of PCN viability achieved by catalase addition to cell medium **(Fig. 2F)** as well as the enhanced sensitivity to BH4 obtained by incubating PCN with 25 μM BSO **(Fig. 2F)**. These results, in line with previous investigations performed with other PD neurotoxins [34] confirm that oxidative stress is the principal event leading to BH4-induced neuronal apoptosis.

BH4 Induces Glycolytic Impairment in Neuronal Cells – Some pieces of evidence from literature suggest a relationship among cellular redox state, glucose metabolism, and neurodegeneration [8, 35]. Therefore, we wondered whether ROS produced downstream of BH4 auto-oxidation could affect cellular energetics. To this aim we focused on the possible impairment of glucose uptake by evaluating the incorporation of 2-NBDG, the fluorescent analogue of deoxy-D-glucose. **Fig. 3A** shows that cells treated for 1 h with 100 μM BH4 exhibited a decrease of 2-NBDG uptake (about -40% with respect to untreated cells). Moreover, if the cells were pre-incubated with 1 μM catalase, no change in 2-NBDG fluorescence was observed, indicating that catalase was able to completely

restore glucose uptake at rates similar to those of control (**Fig. 3A**). We then performed lactate assay in culture media. **Suppl Fig. 3** shows that extracellular lactate, which represents a measure of glycolytic metabolism, significantly decreased after 6 h-treatment with BH4, phenomenon that was completely prevented by pre-incubation with catalase. To confirm a bioenergetic unbalance following glucose uptake inhibition, we monitored phospho-activation of AMPK, an energetic stress-responsive kinase activated downstream of AMP/ATP ratio increase [36]. Despite the basal form of the protein did not change during BH4 treatment (data not shown), Western blot analyses of phosphorylated/activated AMPK (P-AMPK) indicates that it accumulated time-dependently as early as 1h (**Fig. 3B**). Similarly, PCN treated with 1 μM BH4 showed a significant decrease of glucose uptake that was recovered by the addition of catalase (**Fig. 3C**), as well as a time dependent activation of AMPK (**Fig. 3B**). To further investigate whether the ability to impair glucose accumulation was a feature shared with other neurotoxins generating extracellular ROS, we measured 2-NBDG uptake in PCN after 1 h challenge with 5 μM 6-hydroxydopamine (6-OHDA), another redox-cycling molecule. **Fig 3C** shows that, similarly to BH4, also 6-OHDA was able to reduce 2-NBDG accumulation in a ROS-dependent manner. Indeed, the addition of catalase completely restored 2-NBDG uptake suggesting that alterations in glucose homeostasis could contribute to neuronal demise induced by redox-active PD toxins.

p53 is Involved in BH4-Induced Neuronal Apoptosis – To dissect the signaling pathway(s) involved in BH4-induced apoptosis, we focused on p53, whose induction has been correlated with neuronal degeneration. We treated SH-SY5Y cells with 100 μM BH4 and analyzed by Western blot the expression levels of p53 and Bax, one of the well established apoptotic target genes of p53. **Fig. 4A** shows that both proteins were up-regulated as early as 3 h of treatment with BH4, suggesting that p53 accumulation is associated with the acquisition of its nuclear transacting properties. To unravel the role of p53 in BH4-induced cell death, we knocked down p53 expression by transfecting SH-SY5Y cells with two alternative siRNAs against p53 and analyzed apoptotic extent upon treatment with BH4. As shown in **Fig. 4B** and **Suppl. Fig. 4**, the percentage of apoptotic cells was significantly reduced in p53 silenced cells with respect to their non-targeting controls. Moreover, in line with the decreased apoptotic extent, Western blots depicted in **Fig. 4C** show that p53 and Bax were only slightly up-regulated in p53 silenced cells, confirming that p53/Bax axis contributes to BH4 induced apoptosis. To gain insight into the relevance of p53 in BH4-induced cell death, we analyzed its activation in PCN. According to the current view, following its stabilization, p53 translocates into the nucleus in order to activate the transcription of its target genes. Therefore, we analyzed p53 localization in PCN cells upon 24 h-treatment with 1 μM BH4 by means of fluorescence microscopy. **Fig 4D** shows that BH4 challenge induced an increase of nuclear containing p53 cells (+ 36.3 ± 2.5%) with respect to untreated neurons. We inhibited p53 activity with its specific chemical inhibitor pifithrin-α and evaluated apoptosis extent after 24 h-treatment with 1 μM BH4. **Fig. 4E** shows that pre-treatment with 20 μM of pifithrin-α induced a reliable recovery of cell viability, indicating that p53 activation was implicated in the occurrence of BH4-induced apoptosis in primary neurons as well.

$p38^{MAPK}$-mediated Phosphorylative Signaling Responds to BH4 Neurotoxicity – Several studies suggest that two stress-activated protein kinases, JNK and $p38^{MAPK}$, contribute to neuronal demise in many neurodegenerative diseases, being sensitive to ROS production. To elucidate their involvement in BH4-induced SH-SY5Y cells death, we examined their phosphorylation/activation state by Western blot analyses. **Fig.5A** shows that both phospho-$p38^{MAPK}$ and phospho-JNK accumulated upon BH4 treatment. In particular, phospho-$p38^{MAPK}$ rapidly increased as early as 1 h after treatment with BH4, whereas JNK phosphorylation appeared evident only after 3 h. In line with this observation, the phosphorylation state of their downstream transcription factor c-Jun was up-regulated after 3 h of treatment. We next inhibited JNK- and $p38^{MAPK}$-mediated phosphorylative signaling. In particular, **Fig. 5B** shows that pre-treatment with 10 μM of both JNK inhibitor I and II did not protect SH-SY5Y cells from BH4-induced apoptosis, suggesting that JNK phospho-activation was not functional to the apoptotic commitment. By contrast, incubations with 15 μM

SB203580, the selective inhibitor of p38^{MAPK}-upstream kinases MKK3/6, induced a significant recovery of cell viability, indicating that p38^{MAPK} activation was instead implicated in the occurrence of apoptosis. To confirm its involvement in BH4-induced neuronal demise, we then knocked down p38^{MAPK} expression by two alternative siRNAs and analyzed apoptosis after 24 h treatment with BH4. **Fig. 5D** and **Suppl. Fig. 5A** show that sip38^{MAPK} cells were highly resistant to BH4-mediated cell death with respect to their scrambled controls. Similar results were obtained by transfecting the cells with the p38^{MAPK} dominant negative form p38-AF (p38-AF cells), which provides a non-phosphorylable mutant of the α1 subunit of p38^{MAPK} (**Suppl. Fig. 5C**). To corroborate these results, we evaluated the involvement of p38^{MAPK} in apoptotic induction of PCN cells as well. Western blot analyses demonstrated that phospho-p38^{MAPK} accumulated time-dependently as early as 6 h of treatment with 1 μM BH4 **(Fig 5E).** Moreover, its pharmacological inhibition resulted in an almost complete recovery of neurons viability after 24 h challenge with 1 μM BH4 **(Fig. 5F)**, confirming that the engagement of p38^{MAPK}-mediated signaling pathway is fundamental for the neuronal apoptosis induced by BH4.

p38^{MAPK} Activation Contributes to p53 Up-regulation upon BH4 Treatment – p38^{MAPK} can phosphorylate p53 at multiple sites, thus promoting its stabilization and nuclear accumulation in response to various genotoxic stimuli and neurotoxins [14, 37]. Therefore, we investigated the occurrence of a functional connection between these two proteins under our experimental conditions. **Fig. 6A** shows that the silencing of p38^{MAPK} strongly decreased p53 immunoreactive levels upon 3 and 6 h-treatment with BH4. Similar results were obtained both in sip38-2 cells (**Suppl. Fig. 5B**) and in p38-AF cells (**Suppl. Fig. 5D)** indicating that p38^{MAPK} up-regulated p53. To confirm the functional link between p38^{MAPK} and p53 in neurons, we pharmacologically inhibited p38^{MAPK} activation and evaluated p53 localization by fluorescence microscopy after 24 h treatment with 1 μM BH4. **Fig. 6B** shows that, in line with the recovery of neuron viability **(see Fig. 5F)**, pre-treatment with 15 μM of SB203580 induced a consistent decrease of cells displaying nuclear accumulation of p53, indicating that p38^{MAPK}/p53 signaling axis engagement is operative in the occurrence of apoptosis also in neuronal cells.

Oxidative Stress and Glucose Availability Modulate BH4-induced p38^{MAPK}/p53 Signaling Pathway Activation in Neuronal cells – To clarify whether oxidative stress was the upstream event underlying p38^{MAPK}/p53 activation, we pre-incubated SH-SY5Y cells for 12 h with 1 mM BSO. **Fig. 7A** shows that, under these conditions, phospho-p38^{MAPK} and p53 immunoreactive bands resulted enhanced with respect to BH4 treatment alone, confirming that the increase of apoptotic extent, obtained upon GSH depletion (**Fig. 2G**), was associated with the activation of p38^{MAPK}/p53 signaling axis. Moreover, we performed treatments with BH4 in the presence of 1 μM catalase, or upon 12 h-incubation with 5 mM NAC. **Fig. 7B** shows that, consistent with the recovery of cell viability and ROS scavenging (see **Fig. 2F**), catalase and NAC also reduced phospho-p38^{MAPK} and p53 levels after 3 and 6 h of treatment. The involvement of ROS in the activation of p38^{MAPK} and p53 was also found to be operative in PCN. Indeed, catalase decreased the percentage of neurons displaying nuclear accumulation of phospho-p38^{MAPK} and p53 **(Fig.7 C),** confirming that, upon BH4 treatment, the engagement of p38^{MAPK}/p53 pathway is a ROS-dependent event.

To clarify the role of the inhibition of glucose uptake in the sequence of events induced by BH4, we set up growth conditions mimicking glucose deprivation. In particular, we cultured SH-SY5Y cells in 10% of non-essential amino acids and FCS-enriched HBSS medium [24] in the presence (16 mM) or absence of glucose. We then treated the cells with 50 and 100 μM BH4 and analyzed apoptosis cytofluorometrically upon 24 h-treatment. **Fig. 7D** shows that the cells grown in free-glucose conditions were more sensitive to BH4 than those cultured in the presence of glucose. To correlate these effects with the activation of p38^{MAPK}/p53 pathway, we further performed Western blot analyses. **Fig. 7E** shows that phospho-p38^{MAPK} levels and p53 expression significantly increased in conditions of glucose starvation. Glucose restriction was able to modulate viability and the engagement of p38^{MAPK}/p53 signaling axis of PCN as well. In fact, PCN grown in glucose-deprived medium were more sensitive to BH4 treatment (**Fig. 7F**) as well as showed a more

pronounced nuclear localization of phospho-p38^{MAPK} and p53 **(Fig. 7G)** than glucose-feeded counterparts. These results provided evidence for a pivotal role of glucose in the activation of BH4-elicited pro-apoptotic signaling pathway, but a relationship between the extent of oxidative damages and glucose availability was not pointed out yet. To directly examine this issue we analyzed the phospho-activation of the histone H2A.X (P-H2A.X) in condition of glucose deprivation. **Fig. 7H** shows that PCN grown in glucose-free medium displayed a larger amount of discrete P-H2A.X-positive nuclear foci with respect to glucose-feeded neurons, providing a clear-cut evidence for the pivotal role of glucose in the tolerance of neuronal cells to the pro-apoptotic insult elicited after BH4 challenge.

DISCUSSION

BH4 has been suggested to participate in neuronal demise, causing cellular and biochemical alterations consistent with the current view of PD pathogenesis [16-18]: however the molecular mechanisms responsible for its neurotoxic properties remain largely unsolved. In this study we demonstrate that p38^{MAPK} is responsible for the induction of the mitochondrial route of apoptosis both in SH-SY5Y neuroblastoma cells and mouse PCN, through the activation of p53. Our results clearly indicate an increased oxidative damage to proteins and DNA during BH4 exposure. In agreement with its pro-oxidant capacity, BH4 neurotoxicity is attenuated by NAC and completely counteracted by catalase administration confirming, as previously reported in tumor cell lines [32], that H_2O_2, generated during BH4 extracellular redox cycling, is the principal responsible of its toxicity. Moreover, a prominent role in cellular buffering capacity is evidenced for GSH, whose content decreases upon BH4 exposure, as result of BH4-induced oxidative unbalance, and whose chemical depletion enhances the sensitivity of neurons to BH4-mediated cell death. Therefore, on the basis of data from literature indicating GSH decrease as an important pathogenic change in the early stages of PD [38], our results suggest that BH4 acting in the micromolar range, could be an intrinsic factor contributing to neuronal vulnerability, particularly in circumstances predisposing the cells to oxidative insults.

Pro-oxidant conditions occurring upon BH4 administration are responsible for the activation of p38^{MAPK} which is the fundamental mediator of cell death commitment, as demonstrated by a near complete restoration of cell viability obtained silencing its expression and preventing its activation by means of two alternative siRNAs and a non phosphorilable dominant/negative form, respectively. On the other hand, we observe a less significant attenuation of apoptosis when the cells are pre-treated with SB203580, suggesting that the canonical ROS-induced apoptosis signal-regulating kinase 1 (ASK1)-dependent phosphorylation of MKK3/6 pathway is operative, but not exclusive in mediating p38^{MAPK} activation upon BH4 exposure. Moreover, redox unbalance besides promoting p38^{MAPK} activation could contribute to the stabilization of its phosphorylated form, by affecting the activity of the redox-sensitive dual specificity phosphatase 1 (DUSP1). Indeed, the catalytic cysteine of this protein phosphatase has been demonstrated to be oxidized to sulfenic acid upon oxidative conditions, leading to sustained MAPK activation [39]. Furthermore, in line with data from literature showing the ability of p38^{MAPK} to stimulate nuclear translocation of p53 in the ventral midbrain of MPTP-treated mice [14], we point out that, in response to BH4 challenge, p38^{MAPK} mediates p53 phosphorylation and its nuclear accumulation, reinforcing the functional link between these stress responsive proteins in BH4-elicited cell demise. Since p38^{MAPK} has been implicated in the post-transcriptional regulation of a number of genes containing AU-rich regions (AREs) in the 3′ UTR of their mRNAs [40] we could hypothesize a role for p38^{MAPK} in the modulation of p53 mRNA stability, being the p53 mRNA half-life regulated by an ARE-dependent mechanism [41]. However, the only partial attenuation of p53, as a result of p38^{MAPK} inhibition, suggests that other protein kinases or stimuli, could directly contribute to p53 engagement.

Besides relying on the canonical pro-oxidant stimulus, we demonstrate that p38^{MAPK}/p53 signaling axis is responsive to BH4-induced bioenergetic stress elicited by glucose uptake

inhibition, as well. Interestingly, glucose free-medium enhances $p38^{MAPK}$ phosphorylation and p53 activation, which in turn impact on apoptosis commitment. Ongoing investigations from our laboratory indicate AMPK as one of the energy-sensitive serine-threonine protein kinases involved in BH4-induced apoptotic commitment and in the activation of $p38^{MAPK}$/p53 signaling axis in response to reduced glucose availability.

In the sequence of events underlying BH4 toxicity, we point that ROS production is the up-stream event leading to glucose uptake inhibition, as demonstrated by the complete restoration of glucose accumulation achieved in presence of catalase. Although the molecular mechanisms responsible for glucose uptake reduction need to be more deeply dissected, it is reasonable to hypothesize that glucose transporters could be oxidatively affected by BH4-produced ROS. Indeed, it has been reported that facilitative hexose transporters (GLUTs) display conserved cysteine residues lining the extracellular face of the pore, whose bulkier substitutions/modification could affect its size and protein function [42]. However, we cannot rule out the possibility that GLUTs pore could be impaired by irreversible oxidative modifications involving its carbonylation or conjugation with aldehydic by-products of lipid peroxidation, as evidenced in *ex-vivo* models of AD [43]. Beside showing a direct effect of oxidative stress on glucose metabolism, our results provide also the evidence that the extent of BH4-induced oxidative damages and apoptosis is tightly dependent on glucose availability. Similar results were observed by Bolaños and co-workers in rat PCN challenged with glutamate [35]. In that system, the pro-survival effect of glucose seems to rely on the enhancement of the activity of pentose phosphate pathway, which counteracts glutamate-elicited oxidative stress by generating NADPH. Similarly, our findings rise the possibility that the reduced glucose uptake observed in BH4-treated neurons could affect NADPH production, contributing to exacerbate the intrinsic pro-oxidant properties of this molecule.

Our results demonstrate that the ability to impair glucose incorporation in neurons is a feature shared with another well-defined PD neurotoxin, 6-OHDA, able to induce oxidative stress *via* extracellular H_2O_2 generation and $p38^{MAPK}$/p53-dependent neuronal apoptosis [14], similarly to the here identified pathway for BH4 neurotoxicity. Therefore we can hypothesize that the ability to affect glucose availability could be a putative common base for the induction of pro-apoptotic signaling pathways elicited by both 6-OHDA and BH4. Further investigations are ongoing in our laboratory aimed to confirm this assumption on primary dopaminergic neurons, the neuronal population mainly affected in PD.

In conclusion, our study points out that BH4 is of particular hazard for the neural cell integrity, because the oxidative damages deriving from its redox cycles mimic the majority and most established hallmarks of PD. Our results point out that ROS-dependent glucose uptake impairment contributes to BH4-induced neuronal demise through the activation of $p38^{MAPK}$/p53 signaling axis, providing a clear-cut explanation for the citotoxicity of BH4. This study also suggests a role for glucose uptake inhibition in the induction of pro-apoptotic pathways mediated by autoxidizable molecules, in the pathogenesis of neurodegenerative disorders.

REFERENCES

1. Sofic, E., Lange, K.W., Jellinger, K., and Riederer, P. (1992) Reduced and oxidized glutathione in the substantia nigra of patients with Parkinson's disease. Neurosci. Lett. **142**, 128-130
2. Floor, E., and Wetzel, M.G. (1998) Increased protein oxidation in human substantia nigra pars compacta in comparison with basal ganglia and prefrontal cortex measured with an improved dinitrophenylhydrazine assay. J. Neurochem. **70**, 268–275
3. Huang, X., Moir, R.D., Tanzi, R.E., Bush, A.I., and Rogers J.T. (2004) Redox-active metals, oxidative stress, and Alzheimer's disease pathology. Ann N Y Acad Sci. **1012**, 153-163
4. de Leon, M.J., Ferris, S.H., George, A.E., Christman, D.R., Fowler, J.S., Gentes, C., Reisberg, B., Gee, B., Emmerich, M., Yonekura, Y., Brodie, J., Kricheff, I.I., and Wolf, A.P. (1983)

Positron emission tomographic studies of aging and Alzheimer disease. AJNR Am. J. Neuroradiol. **4**, 568–571

5. Ma, Y., and Eidelberg, D. (2007) Functional imaging of cerebral blood flow and glucose metabolism in Parkinson's disease and Huntington's disease. Mol. Imaging. Biol. **9**, 223-233
6. Arias, C., Montiel, T., Quiroz-Baez, R., and Massieu, L. (2002) beta-Amyloid neurotoxicity is exacerbated during glycolysis inhibition and mitochondrial impairment in the rat hippocampus in vivo and in isolated nerve terminals: implications for Alzheimer's disease. Exp. Neurol. **176**, 163–174
7. Bellucci, A., Collo, G., Sarnico, I., Battistin, L., Missale, C., and Spano, P. (2008) Alpha-synuclein aggregation and cell death triggered by energy deprivation and dopamine overload are counteracted by D2/D3 receptor activation. J Neurochem **106**, 560-577
8. Gandhi, S., Wood-Kaczmar, A., Yao, Z., Plun-Favreau, H., Deas, E., Klupsch, K., Downward, J., Latchman, D.S., Tabrizi, S.J., Wood, N.W., Duchen, M.R., and Abramov, A.Y. (2009) PINK1-associated Parkinson's disease is caused by neuronal vulnerability to calcium-induced cell death. Mol. Cell **33**, 627-638
9. Perier, C., Bové, J., Wu, D.C., Dehay, B., Choi, D.K., Jackson-Lewis, V., Rathke-Hartlieb, S., Bouillet, P., Strasser, A., Schulz, J.B., Przedborski, S., and Vila, M. (2007) Two molecular pathways initiate mitochondria-dependent dopaminergic neurodegeneration in experimental Parkinson's disease. Proc. Natl. Acad. Sci. USA **104**, 8161–8166
10. Duan, W., Zhu, X., Ladenheim, B., Yu, Q.S., Guo, Z., Oyler, J., Cutler, R.G., Cadet, J.L., Greig, N.H., and Mattson, M.P. (2002) p53 inhibitors preserve dopamine neurons and motor function in experimental parkinsonism. Ann. Neurol. **52**, 597-606.
11. Trimmer, P.A., Smith, T.S., Jung, A.B., and Bennett, J.P. Jr. (1996) Dopamine neurons from transgenic mice with a knockout of the p53 gene resist MPTP neurotoxicity. Neurodegeneration **5**, 233-239
12. Gomez-Lazaro, M., Galindo, M.F., Concannon, C.G., Segura, M.F., Fernandez-Gomez, F.J., Llecha, N., Comella, J.X., Prehn, J.H., and Jordan, J. (2008) 6-Hydroxydopamine activates the mitochondrial apoptosis pathway through p38 MAPK-mediated, p53-independent activation of Bax and PUMA J. Neurochem. **104**, 1599-1612
13. Savage, M.J., Lin, Y.G., Ciallella, J.R., Flood, D.G., and Scott, R.W. (2002) Activation of c-Jun N-terminal kinase and p38 in an Alzheimer's disease model is associated with amyloid deposition. J Neurosci. **22**, 3376-3385
14. Karunakaran, S., Saeed, U., Mishra, M., Valli, R.K., Joshi, S.D., Meka, D.P., Seth, P., and Ravindranath, V. (2008) Selective activation of p38 mitogen-activated protein kinase in dopaminergic neurons of substantia nigra leads to nuclear translocation of p53 in 1-methyl-4-phenyl-1,2,3,6-tetrahydropyridine-treated mice. J. Neurosci. **28**, 12500-12509
15. Choi, H.J., Kim, S.W., Lee, S.Y., and Hwang, O. (2003) Dopamine-dependent cytotoxicity of tetrahydrobiopterin: a possible mechanism for selective neurodegeneration in Parkinson's disease. J. Neurochem. **86,** 143-152
16. Lee, S.Y., Moon, Y., Hee Choi, D., Jin Choi, H., and Hwang, O. (2007) Particular vulnerability of rat mesencephalic dopaminergic neurons to tetrahydrobiopterin: Relevance to Parkinson's disease. Neurobiol. Dis. **25**, 112-120
17. Kim, S.W., Jang, Y.J., Chang, J.W., and Hwang, O. (2003) Degeneration of the nigrostriatal pathway and induction of motor deficit bytetrahydrobiopterin: an in vivo model relevant to Parkinson's disease. Neurobiol. Dis. **13**, 167-176
18. Kim, S.T., Chang, J.W., Hong, H.N., and Hwang, O. (2004) Loss of striatal dopaminergic fibers after intraventricular injection of tetrahydrobiopterin in rat brain. Neurosci. Lett. **359,** 69-72
19. Levine, R.A., Miller, L.P., and Lovenberg, W. (1981) Tetrahydrobiopterin in striatum: localization in dopamine nerve terminals and role in catecholamine synthesis. Science **214**, 919-21

20. Hwang, O., Choi, H.J., and Park, S.Y. (1999) Up-regulation of GTP cyclohydrolase I and tetrahydrobiopterin by calcium influx. NeuroReport **10**, 3611-3614
21. Kim, S.T., Chang, J.W., Choi, J.H., Kim, S.W., and Hwang, O. (2005) Immobilization stress causes increases in tetrahydrobiopterin, dopamine, and neuromelanin and oxidative damage in the nigrostriatal system. J. Neurochem. **95**, 89-98
22. Cho, S., Volpe, B.T., Bae, Y., Hwang, O., Choi, H.J., Gal, J., Park, L.C., Chu, C.K., Du, J., and Joh, T.H. (1999) Blockade of tetrahydrobiopterin synthesis protects neurons after transient forebrain ischemia in rat: a novel role for the cofactor. J. Neurosci. **19**, 878–889
23. Kirsch, M., Korth, H.G., Stenert, V., Sustmann, R., and de Groot, H. (2003) The autoxidation of tetrahydrobiopterin revisited. Proof of superoxide formation from reaction of tetrahydrobiopterin with molecular oxygen. J. Biol. Chem. **278**, 24481-24490
24. Bellucci, A., Collo, G., Sarnico, I., Battistin, L., Missale, C., and Spano, P. (2008) Alpha-synuclein aggregation and cell death triggered by energy deprivation and dopamine overload are counteracted by D2/D3 receptor activation. J. Neurochem. **106**, 560-577
25. Filomeni, G., Cerchiaro, G., Da Costa Ferreira, A.M., De Martino, A., Pedersen, J.Z., Rotilio, G., and Ciriolo, M.R. (2007) Pro-apoptotic activity of novel Isatin-Schiff base copper(II) complexes depends on oxidative stress induction and organelle-selective damage. J. Biol. Chem. **282**, 12010-12021
26. Nicoletti, I., Migliorati, G., Pagliacci, M.C., Grignani, F., and Riccardi, C. (1991) A rapid and simple method for measuring thymocyte apoptosis by propidium iodide staining and flow cytometry. J. Immunol. Methods **139**, 271-279
27. Filomeni, G., Rotilio, G., and Ciriolo, M.R. (2003) Glutathione disulfide induces apoptosis in U937 cells by a redox-mediated p38 MAP kinase pathway.FASEB J. **17**, 64-66
28. Filomeni, G., Aquilano, K., Rotilio, G., and Ciriolo, M.R. (2003) Reactive oxygen species-dependent c-Jun NH2-terminal kinase/c-Jun signaling cascade mediates neuroblastoma cell death induced by diallyl disulfide. Cancer Res. **63**, 5940-5949
29. Cardaci, S., Filomeni, G., Rotilio, G., and Ciriolo, M.R. (2008) Reactive oxygen species mediate p53 activation and apoptosis induced by sodium nitroprusside in SH-SY5Y cells. Mol. Pharmacol. **74**, 1234-1245
30. Filomeni, G., Desideri, E., Cardaci, S., Graziani, I., Piccirillo, S., Rotilio, G., and Ciriolo M.R. (2010) Carcinoma cells activate AMP-activated protein kinase-dependent autophagy as survival response to kaempferol-mediated energetic impairment. Autohagy **6**, in press.
31. Lowry, O.H., Rosebrough, N.J., Farr, A.L., and Randall, R.J. (1951) Protein measurement with the Folin phenol reagent. J. Biol. Chem. **193**, 265-275
32. Choi, H.J., Jang, Y.J., Kim, H.J., and Hwang, O. (2000) Tetrahydrobiopterin is released from and causes preferential death of catecholaminergic cells by oxidative stress. Mol. Pharmacol. **58**, 633-640
33. Chongthammakun, V., Sanvarinda, Y., and Chongthammakun, S. (2009) Reactive oxygen species production and MAPK activation are implicated in tetrahydrobiopterin-induced SH-SY5Y cell death. Neurosci. Lett. **449**, 178-182
34. Nakamura, K., Wang, W., and Kang, U.J. (1997) The role of glutathione in dopaminergic neuronal survival. J. Neurochem. **69**, 1850-1858
35. Delgado-Esteban, M., Almeida, A., and Bolaños, J.P. (2000) D-Glucose prevents glutathione oxidation and mitochondrial damage after glutamate receptor stimulation in rat cortical primary neurons. J. Neurochem. **75**, 1618-1624
36. Hardie, D.G. (2007) AMP-activated/SNF1 protein kinases: conserved guardians of cellular energy. Nat. Rev. Mol. Cell. Biol. **8**, 774-785
37. Piccirillo, S., Filomeni, G., Brüne, B., Rotilio, G., Ciriolo, M.R. (2009) Redox mechanisms involved in the selective activation of Nrf2-mediated resistance versus p53-dependent apoptosis in adenocarcinoma cells. J. Biol. Chem. **284**, 27721-27733

38. Sian, J., Dexter, D.T., Lees, A.J., Daniel, S., Agid, Y., Javoy-Agid, F., Jenner, P., and Marsden, C.D. (1994) Alterations in glutathione levels in Parkinson's disease and other neurodegenerative disorders affecting basal ganglia. Ann. Neurol. **36**, 348-355
39. Kamata, H., Honda, S., Maeda, S., Chang, L., Hirata, H., and Karin, M. (2005) Reactive oxygen species promote TNFalpha-induced death and sustained JNK activation by inhibiting MAP kinase phosphatases. Cell. **120**, 649-661.
40. Frevel, M.A.E., Bakheet, T., Silva, A.M., Hissong, J.G., Khabar, K.S.A., and Williams B.R.G. (2003**)** p38 mitogen-activated protein kinase-dependent and -independent signaling of mRNA stability of AU-rich element-containing transcripts. Mol Cell Biol. 23, 425-436
41. Vilborg, A., Glahder, J.A., Wilhelm, M.T., Bersani, C., Corcoran, M., Mahmoudi, S., Rosenstierne, M., Grandér, D., Farnebo, M., Norrild, B., and Wiman, K.G. (2009) The p53 target Wig-1 regulates p53 mRNA stability through an AU-rich element. Proc Natl Acad Sci U S A. 106, 15756-15761.
42. Simpson, I.A., Dwyer, D., Malide, D., Moley, K.H., Travis, A., and Vannucci, S.J. (2008) The facilitative glucose transporter GLUT3: 20 years of distinction. *Am J Physiol Endocrinol Metab* **295:** 242-253.Am. J. Physiol. Endocrinol. Metab. **295**, 242-253
43. Mark, R.J.**,** Pang, Z., Geddes, J.W.**,** Uchida, K.**,** and Mattson**,** M.P. (1997) Amyloid beta-peptide impairs glucose transport in hippocampal and cortical neurons: involvement of membrane lipid peroxidation. J. Neurosci. **17,** 1046-1054

FOOTNOTES

We gratefully acknowledge Palma Mattioli for her technical assistance in fluorescence microscopy and image analyses .This work was partially supported by grants from Ministero dell'Università e della Ricerca Scientifica (MIUR) and Ministero della Salute.

ABBREVIATIONS

AMPK, AMP-activated protein kinase; ASK1, apoptosis signal-regulating kinase 1; BH4, tetrahydrobiopterin; BSO, Buthionine sulfoximine; DAF-DA, 4,5-diaminofluorescein diacetate; DCFH-DA, 2',7'-dichlorodihydrofluorescein diacetate; DMEM, Dulbecco's modified Eagle's medium; DMSO, dimethyl sulfoxide; DNP, 2,4-dinitrophenylhydrazine; DTT, dithiotreitol; GLUT, glucose/hexose transporter; GSH, reduced glutathione; GSSG, glutathione disulfide; 6-OHDA, 6-hydroxydopamine; JNK, c-Jun-N-terminal kinase; L-NAME, N(G)-nitro-L-arginine methyl ester; MAPK, mitogen activated protein kinase; MPTP, 1-methyl-4-phenyl-1,2,3,6-tetrahydropyridine; NAC, N-acetylcysteine; 2-NBDG, 2-[N-(7-nitrobenz-2-oxa-1,3-diazol-4-yl) amino]-2-deoxy-D-glucose; 7-Ni, 7-nitroindazole; NO, nitric oxide; NOS, nitric oxide synthase; PARP, polyADP-ribose polymerase; PCN, primary cortical neurons; PD, Parkinson's disease; PINK1, PTEN-induced putative kinase 1; ROS, reactive oxygen species; siRNA, small interference RNA; zVAD-*fmk*, benzyloxycarbonyl-Val-Ala-Asp-fluoromethyl ketone.

DISCLOSURE STATEMENTS

The authors declare no actual or potential conflicts of interest.

FIGURE LEGENDS

Figure 1. *BH4 induces apoptosis in neuronal cells.* **A.** SH-SY5Y cells were treated with 50-200 μM BH4 for 24 h, washed and stained with propidium iodide. Analysis of cell cycle and apoptosis were performed by a FACScalibur instrument and percentages of staining-positive cells were calculated using WinMDI version 2.8 software. Cell cycle plots reported are from a typical experiment done in triplicate out of five that gave similar results. **B.** SH-SY5Y were treated with 100 μM BH4. At the indicated times, cells were lysed and 30 μg of total cell extracts were loaded for the immuno-detection of caspase-9, caspase-3 and PARP. Actin was used as loading control. Immunoblots are from one experiment representative of three that gave similar results. *cl. PARP*, cleaved PARP. PCN were treated with 1-50 μM BH4 for 24 h,washed, fixed in 4% paraformaldehyde and permeabilized. Cleaved caspase-3 was visualized upon staining with a specific antibody and further probed with Alexa fluor®-568-conjugated secondary antibody. To visualize nuclei, cells were also incubated with the cell permeable DNA dye Hoechst 33342. Representative images (**C**.) and the percentages of cells with apoptotic nuclei and cleaved caspase-3 are shown (**D**.). Values represent the mean ± S.D (n = 5). **, $p < 0.01$; ***, $p < 0.001$.

Figure 2. *BH4 elicits oxidative stress in neuronal cells.* **A.** SH-SY5Y cells were treated with 100 μM BH4 for 30 min, 1 or 3 h, and incubated with 50 μM DCF-DA at 37 °C. At indicated time points, cells were washed with PBS and ROS production was analyzed by FACScalibur instrument. Histograms shown are representative of three experiments that gave similar results. **B.** SH-SY5Y cells were treated with 100 μM BH4. At the indicated times, cells were collected, exhaustively washed with PBS and used for GSH and GSSG assay by HPLC. Data are expressed as nmoles of GSH or GSSG/mg total proteins and represent the mean ± S.D (n = 5). For GSH: *, $p < 0.05$; **, $p < 0.01$. For GSSG: $^{\#}$, $p < 0.05$; $^{\#\#}$, $p < 0.01$. **C.** SH-SY5Y cells were treated with 100 μM BH4. At the indicated times, cells were fixed with *p*-formaldehyde and subjected to immunostaining with an anti-phospho-H2A.X antibody (*P-H2A.X*) and further probed with Alexa fluor®-488-conjugated secondary antibody. Nuclei were stained with Hoechst 33342. Images reported are from one experiment of three that gave similar results. SH-SY5Y cells were treated with 100 μM BH4 upon 12 h-incubation with 5 mM NAC or in the presence of 1 μM catalase (**D**), or with 1 mM BSO (**E**). After 3 h cells were incubated for further 30 min with 50 μM DCF-DA at 37 °C, washed with PBS and ROS production was analyzed by FACScalibur instrument. Data are expressed as % DCF^{+} cells. After 24 h cells were stained with propidium iodide. Analysis of subG1 (apoptotic) cells was performed by a FACScalibur instrument. Data are expressed as % of apoptosis. Values represent the mean ± S.D (n = 5). **, $p < 0.01$; ***, $p < 0.001$. **F.** PCN were treated with 1 μM BH4 in the presence of 1 μM catalase, or with 1 mM BSO. After 24 h cells were stained with Hoechst 33342 and condensed or fragmented nuclei were counted as apoptotic. Data are expressed as % of apoptotic nuclei. Values represent the mean ± S.D (n = 5). *, $p < 0.05$; ***, $p < 0.001$.

Figure 3. *BH4 induces glucose uptake inhibition.* **A.** SH-SY5Y cells were treated with 100 μM BH4 for 1 h in the presence or absence of 1 μM catalase and replaced with fresh medium containing 100 μM 2-NBDG. After 15, 30 and 60 min, cells were washed to stop 2-NBDG uptake, collected and fluorescence analyzed cytofluorometrically. Data are expressed as percentage of decrease with respect to untreated (control) cells and represent the mean ± S.D. n = 6, **$p < 0.01$; *** $p < 0.001$. **B.** SH-SY5Y cells and PCN were treated respectively with 100 μM and 1 μM BH4. At the indicated times, cells were lysed and 30 μg of total cell extracts were loaded for the immuno-detection of phospho-activated form of AMPK. GAPDH was used as loading control. Immunoblots are from one experiment representative of three that gave similar results. **C.** PCN were treated with 1μM BH4, or, alternatively, 5 μM 6-OHDA in the presence or absence of 1 μM catalase. After 30 min, 2-NBDG fluorescence was analyzed cytofluorometrically. Data are expressed as percentage of

decrease with respect to untreated (control) cells and represent the mean ± S.D. n = 6. BH4 or 6-OHDA treated cells *versus* control, *$p < 0.05$; *versus* catalase co-administration $^{\#}p < 0.05$.

Figure 4. *p53 activation is functional for BH4-induced apoptosis.* **A.** SH-SY5Y were treated with 100 μM BH4. At the indicated times, cells were lysed and 30 μg of total cell extracts were loaded for the immuno-detection of p53 and Bax. Actin was used as loading control. Immunoblots are from one experiment representative of three that gave similar results. **B.** SH-SY5Y cells were transiently transfected with siRNA duplex directed against the p53 mRNA target sequence (sip53) or with a scramble siRNA duplex (siScr), which does not present homology with any other human mRNAs. Cell adhesion has been allowed for 12 h, then the cells were treated with 100 μM BH4 for the next 24 h, washed and stained with propidium iodide for the detection of apoptotic cells. Data are expressed as % of apoptosis and represent the mean ± S.D. n = 6, *$p < 0.05$. **C.** After 12 h from transfection with siScr or sip53, SH-SY5Y cells were treated with 100 μM BH4. At the indicated times, cells were lysed and 30 μg of total cell extracts were loaded for the immuno-detection of p53 and Bax. Actin was used as loading control. Immunoblots are from one experiment representative of three that gave similar results. **D.** PCN were treated with 1 μM BH4 for 24 h,washed, fixed in 4% paraformaldehyde and permeabilized. p53 was visualized upon staining with specific antibody and further probed with Alexa fluor®-568-conjugated secondary antibody. Nuclei were visualized by incubation with Hoechst 33342. Images reported are from one experiment of three that gave similar results. White arrows indicate representative cells where anti-p53 and Hoechst fluorescences superimpose. **E.** PCN were treated with 1 μM BH4 in the presence or absence of 20 μM pifithrin-α. After 24 h cells were stained with Hoechst 33342 and condensed or fragmented nuclei were counted as apoptotic. Data are expressed as % of apoptotic nuclei. Values represent the mean ± S.D (n = 5). **, $p < 0.01$.

Figure 5. *$p38^{MAPK}$ activation mediates BH4-induced apoptosis.* **A.** SH-SY5Y were treated with 100 μM BH4. At the indicated times, cells were lysed and 30 μg of total cell extracts were loaded for the immuno-detection of basal and phospho-activated forms of $p38^{MAPK}$ and JNK, as well as phospho-c-Jun. GAPDH was used as loading control. Immunoblots are from one experiment representative of three that gave similar results. **B.** SH-SY5Y were incubated for 1 h with 10 μM of the JNK inhibitor I and II, 15 μM of the $p38^{MAPK}$ inhibitor SB203580, or with vehicle alone, then were treated with 100 μM BH4. After 24 h they were washed and stained with propidium iodide for the detection of apoptotic cells. Data are expressed as % of apoptosis and represent the mean ± S.D. n = 6, **$p < 0.01$. **C.** SH-SY5Y cells were transiently transfected with SignalSilence® Pool $p38^{MAPK}$ siRNA ($sip38^{MAPK}$) or with a scramble siRNA duplex (siScr). Cell adhesion has been allowed for 12 h, then the cells were treated with 100 μM BH4. At the indicated times, cells were lysed and 30 μg of total cell extracts were loaded for the immuno-detection of basal and phospho-activated forms of $p38^{MAPK}$. GAPDH was used as loading control. Immunoblots are from one experiment representative of three that gave similar results. **D.** After 12 h from adhesion, $sip38^{MAPK}$ or siScr cells were treated with 100 μM BH4 for the next 24 h, washed and stained with propidium iodide for the detection of apoptotic cells. Data are expressed as % of apoptosis and represent the mean ± S.D. n = 6, ***$p < 0.001$. **E.** PCN were treated with 1 μM BH4. At the indicated times, cells were lysed and 30 μg of total cell extracts were loaded for the immuno-detection of the phospho-activated forms of $p38^{MAPK}$. GAPDH was used as loading control. Immunoblots are from one experiment representative of three that gave similar results. **F.** PCN were treated with 1 μM BH4 in the presence or absence of 15 μM SB203580. After 24 h cells were stained with Hoechst 33342 and condensed or fragmented nuclei were counted as apoptotic. Data are expressed as % of apoptotic nuclei. Values represent the mean ± S.D (n = 5). **, $p < 0.01$.

Figure 6. *p38^{MAPK} regulates p53 activation.* **A.** SH-SY5Y cells were transiently transfected with SignalSilence® Pool p38^{MAPK} siRNA (sip38^{MAPK}) or with a scramble siRNA duplex (siScr). Cell adhesion has been allowed for 12 h, then the cells were treated with 100 μM BH4. At the indicated times, cells were lysed and 30 μg of total cell extracts were loaded for the immuno-detection of phospho-p38^{MAPK} and p53. GAPDH was used as loading control. Immunoblots are from one experiment representative of three that gave similar results. **B.** sip38^{MAPK} and siScr cells were treated with 100 μM BH4 for 6h,washed, fixed in 4% paraformaldehyde and permeabilized. Phospho-p38^{MAPK} and p53 were visualized upon staining with specific antibodies and further probed with Alexa fluor®-488 and Alexa fluor®-568-conjugated secondary antibodies, respectively. To visualize nuclei, cells were also incubated with the cell permeable DNA dye Hoechst 33342. Images reported are from one experiment of three that gave similar results. **C.** PCN were treated with 1 μM BH4 in the presence of 15 μM SB203580. After 24 h cells were washed, fixed in 4% paraformaldehyde and subjected to immunostaining with an anti-p53 antibody and further probed with Alexa fluor®-568-conjugated secondary antibody. Nuclei were stained with Hoechst 33342. Quantitative analyses of cells displaying nuclear p53 localization are shown. Values represent the mean ± S.D (n = 5). *, $p < 0.05$.

Figure 7. *BH4-produced ROS and glucose availability influence p38^{MAPK}/p53 signaling axis activation.* **A.** SH-SY5Y cells were treated with 50 or 100 μM BH4 upon 12 h-incubation with 1 mM BSO. After 6 h cells were lysed and 30 μg of total cell extracts were loaded for the immuno-detection of phospho-p38^{MAPK} and p53. GAPDH was used as loading control. Immunoblots are from one experiment representative of three that gave similar results. **B.** SH-SY5Y cells were treated with 100 μM BH4 upon 12 h-incubation with 5 mM NAC or in the presence of 1 μM catalase. After 3 and 6 h cells were lysed and 30 μg of total cell extracts were loaded for the immuno-detection of phospho-p38^{MAPK} and p53. GAPDH was used as loading control. Immunoblots are from one experiment representative of three that gave similar results. **C.** PCN were treated with 1 μM BH4 in the presence of 15 μM SB203580. After 24 h cells were washed, fixed in 4% paraformaldehyde and subjected to immunostaining with an anti-p53 antibody or, alternatively, with an anti phospho-p38^{MAPK} antibody and further probed with Alexa fluor®-568-conjugated secondary antibody. Nuclei were stained with Hoechst 33342. Quantitative analyses of cells displaying nuclear p53 localization or p38^{MAPK} phospho-activation are shown. Values represent the mean ± S.D (n = 5). **, $p < 0.01$. **D.** SH-SY5Y were treated with 50 or 100 μM BH4 in HBSS supplemented with 10% FCS, 0.01 mM non-essential amino acids, 1% glutamine with or without glucose. After 24 h cells were washed and stained with propidium iodide for the detection of apoptotic cells. Data are expressed as % of apoptosis and represent the mean ± S.D .n = 4, $**p < 0.01$. **E.** SH-SY5Y were treated with 100 μM BH4 in HBSS supplemented with 10% FCS and non-essential amino acids with or without glucose. At the indicated times, cells were lysed and 30 μg of total cell extracts were loaded for the immuno-detection of phospho-p38^{MAPK} and p53. GAPDH was used as loading control. Immunoblots are from one experiment representative of three that gave similar results. Similarly, PCN were treated with 1 μM BH4 in HBSS supplemented with B27, 0.01 mM non-essential amminoacids, 1% glutamine with or without glucose. After 24 h cells were washed, fixed in 4% paraformaldehyde and subjected to immunostaining with an anti-p53 antibody or, alternatively, with an anti phospho-p38^{MAPK} antibody and further probed with Alexa fluor®-568-conjugated secondary antibody. Nuclear damage was evaluated by means of immunostaining with an anti-phospho-H2A.X antibody, further probed with Alexa fluor®-488-conjugated secondary antibody. Nuclei were stained with Hoechst 33342. The percentages of cells displaying apoptotic nuclei (**F**), nuclear p53 localization and p38^{MAPK} phospho-activation (**G**), as well as discrete P-H2A.X nuclear foci (**H**) are shown. Values represent the mean ± S.D (n = 5). *, $p < 0.05$.

Biochemical Journal Immediate Publication. Published on 30 Jun 2010 as manuscript BJ20100503

Figure 1

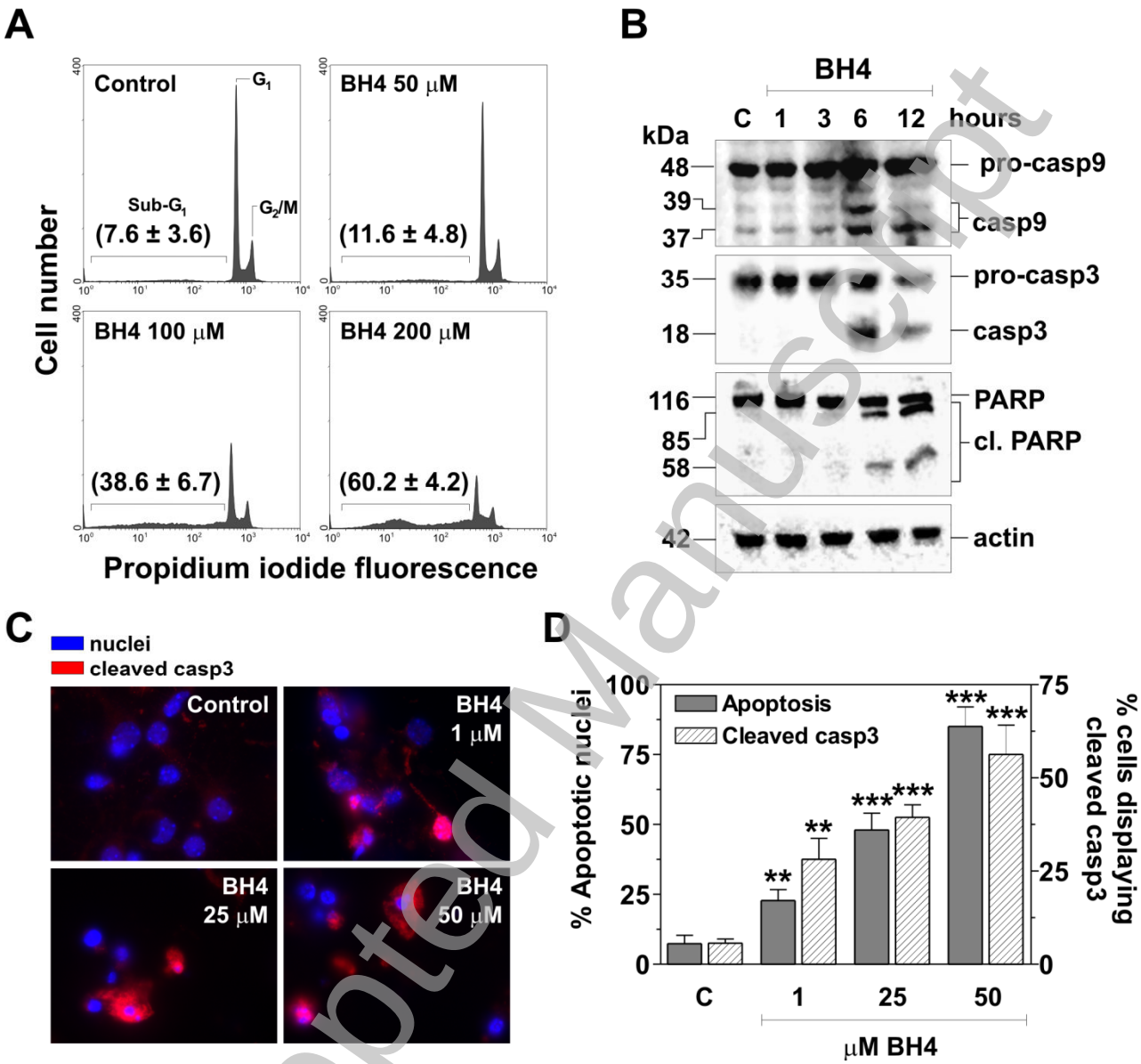

Biochemical Journal Immediate Publication. Published on 30 Jun 2010 as manuscript BJ20100503

Figure 2

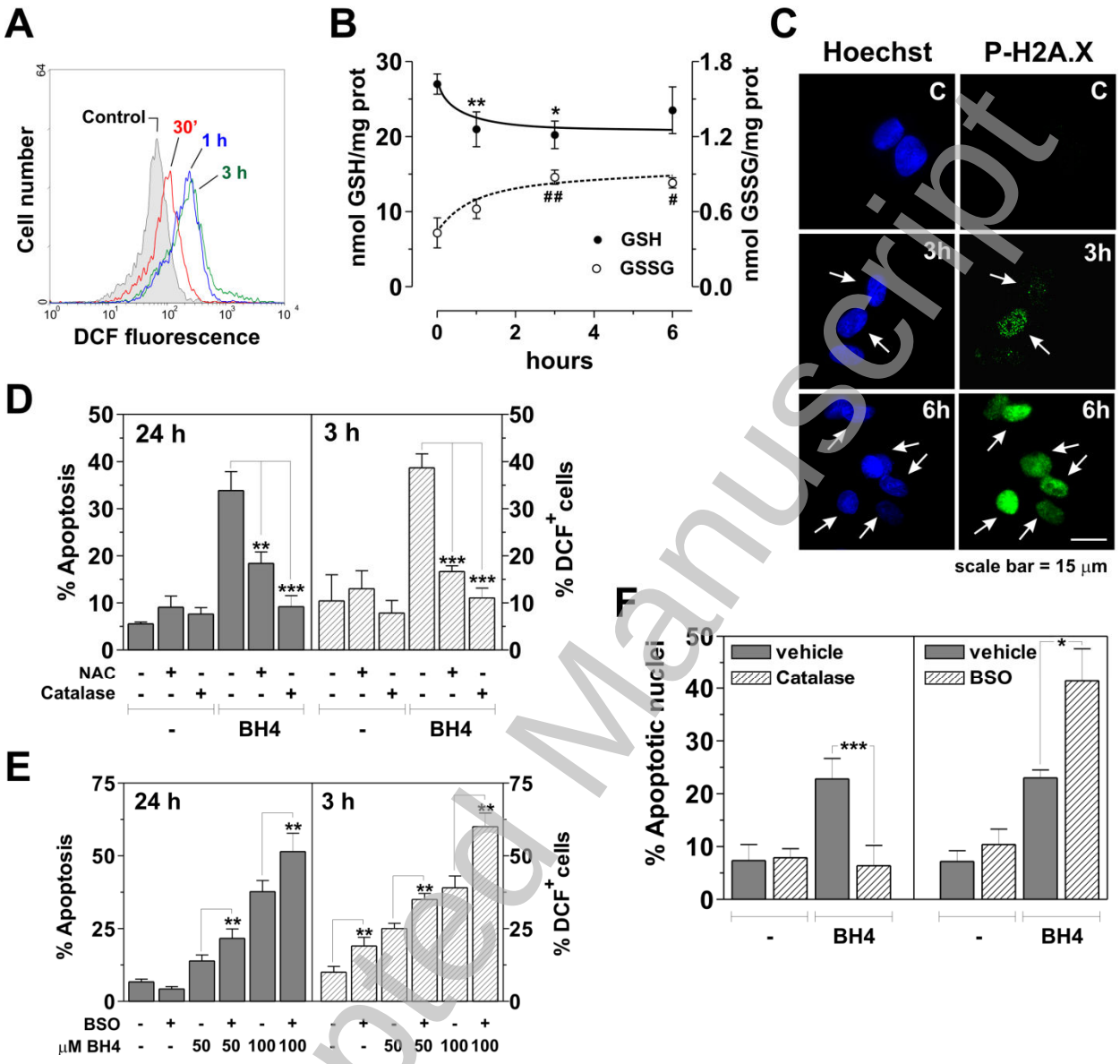

Biochemical Journal Immediate Publication. Published on 30 Jun 2010 as manuscript BJ20100503

Figure 3

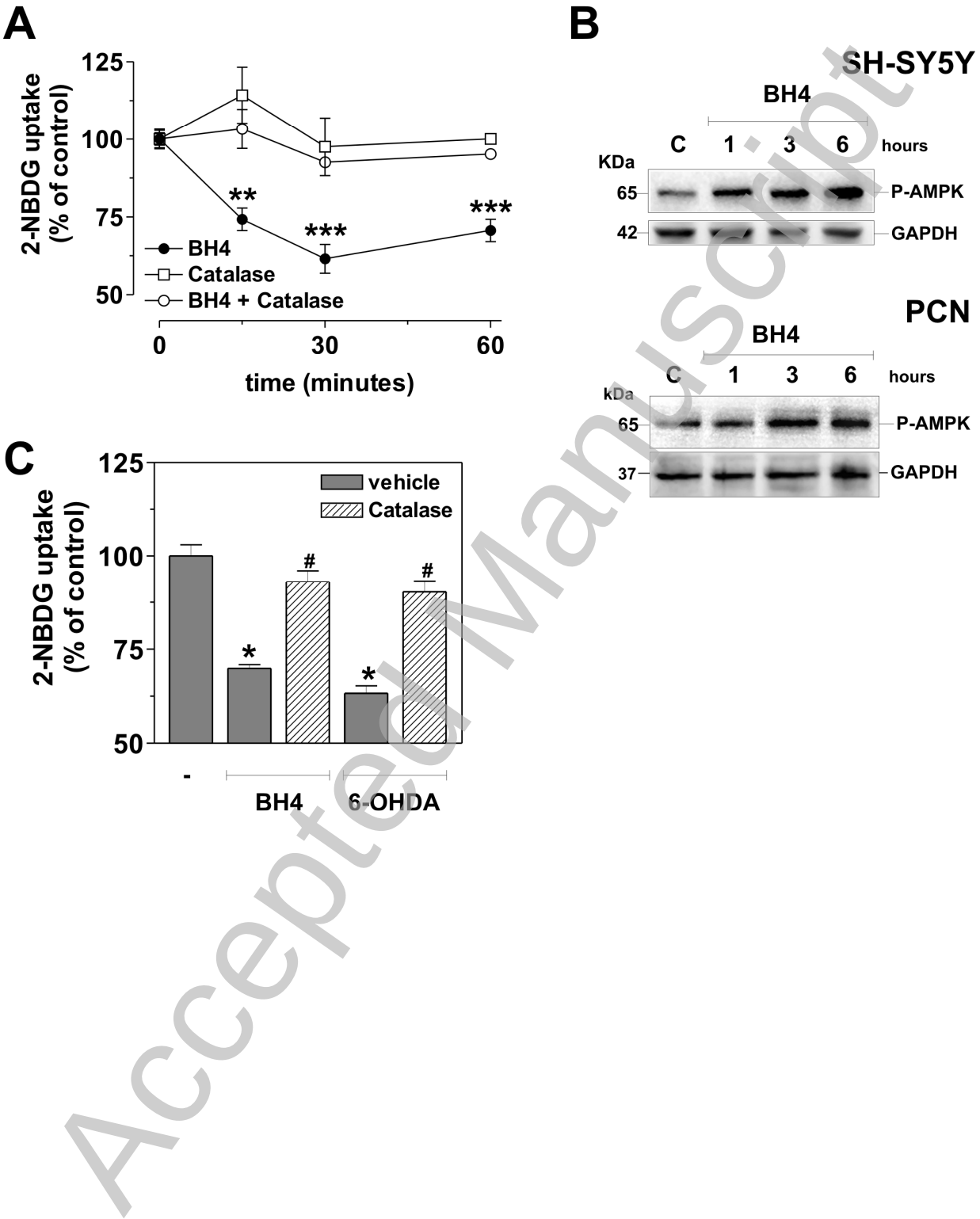

Biochemical Journal Immediate Publication. Published on 30 Jun 2010 as manuscript BJ20100503

Figure 4

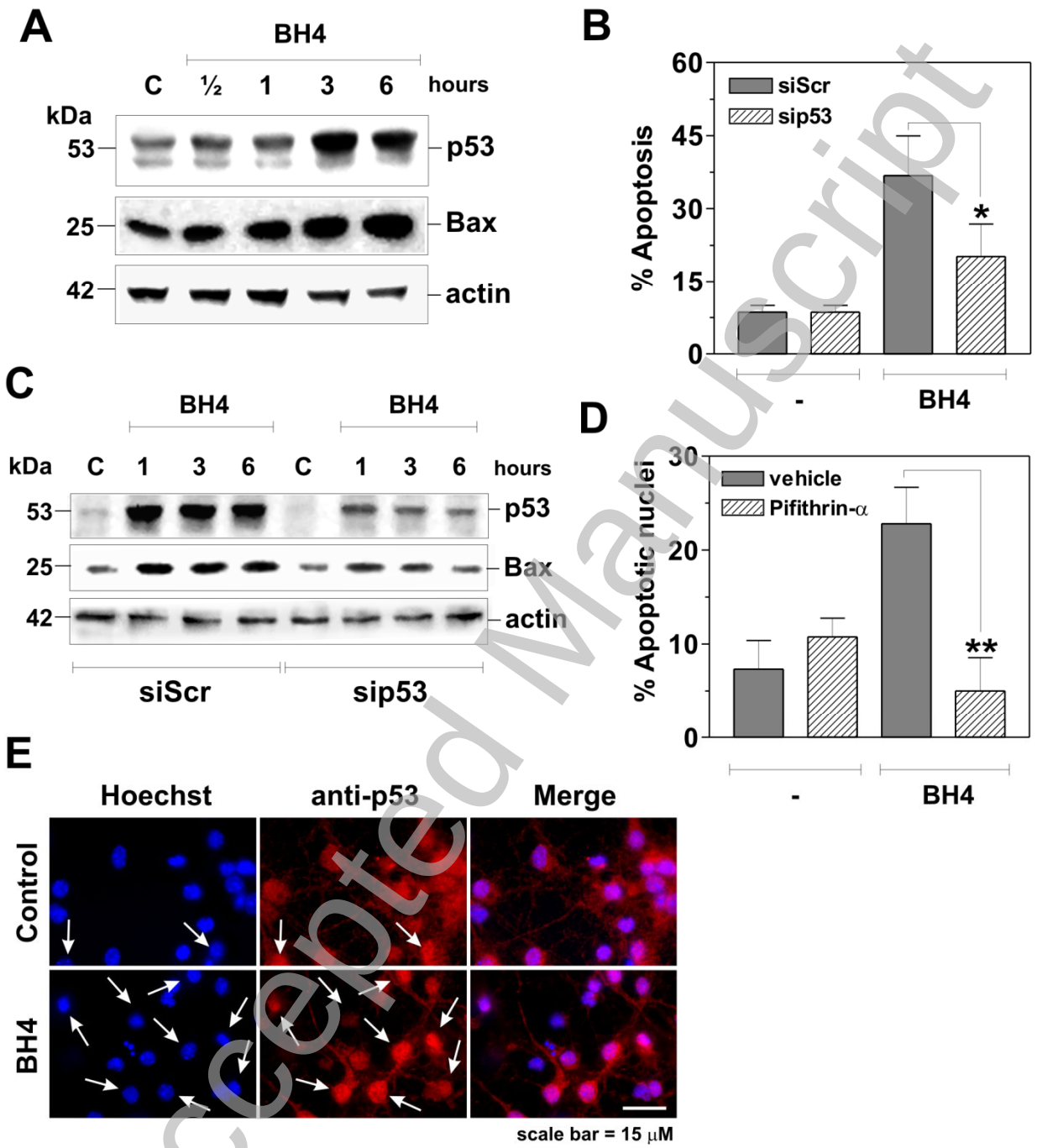

Biochemical Journal Immediate Publication. Published on 30 Jun 2010 as manuscript BJ20100503

Figure 5

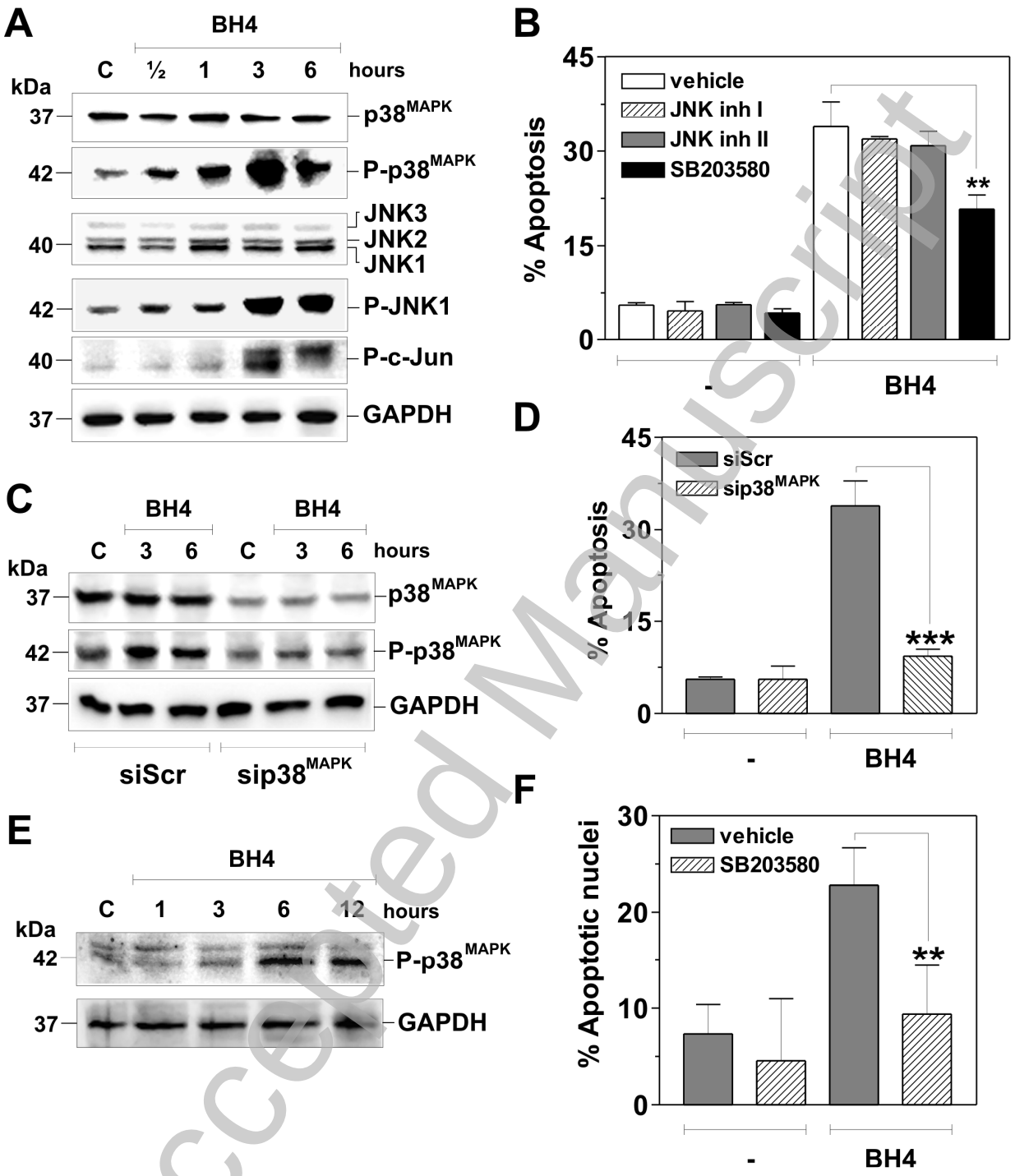

Biochemical Journal Immediate Publication. Published on 30 Jun 2010 as manuscript BJ20100503

Figure 6

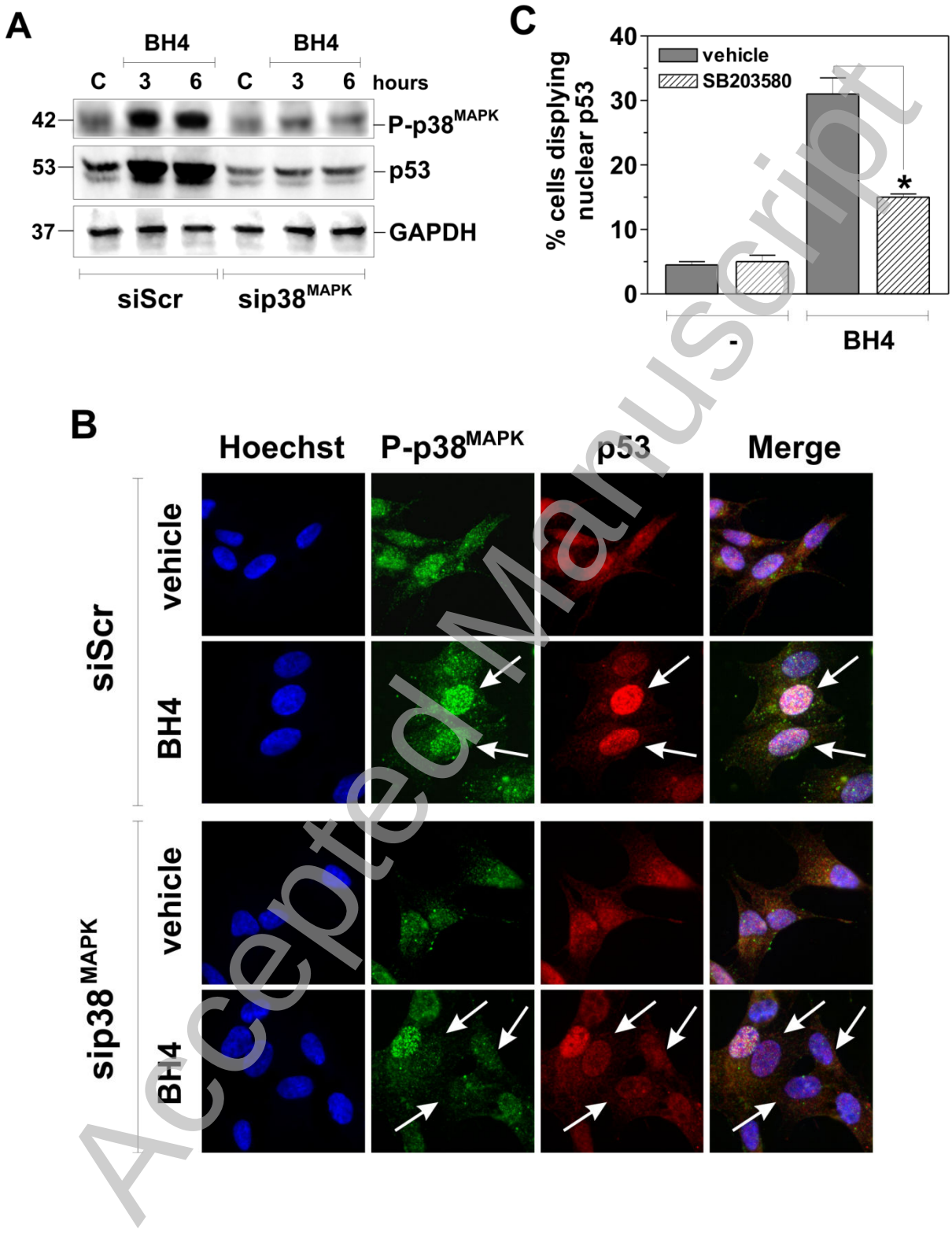

Biochemical Journal Immediate Publication. Published on 30 Jun 2010 as manuscript BJ20100503

Figure 7